LAWRENCE
LIVERMORE
NATIONAL
LABORATORY

UCRL-JRNL-212020

High temperature stability multilayers for EUV condenser optics

S. Bajt, D. G. Stearns

May 6, 2005

Applied Optics

High Temperature Stability Multilayers for EUV Condenser Optics

Saša Bajt[a] and D. G. Stearns[b]

[a]Lawrence Livermore National Laboratory, 7000 East Avenue, Livermore, CA 94550, USA,

[b]OS Associates, Mountain View, CA 94040, USA

We investigate the thermal stability of Mo/SiC multilayer coatings at elevated temperatures. Transmission electron microscopy and x-ray diffraction studies show that upon annealing a thermally-induced structural relaxation occurs that transforms the polycrystalline Mo and amorphous SiC layers in as-deposited multilayers into amorphous Mo-Si-C alloy and crystalline SiC, respectively. After this relaxation process is complete the multilayer is stable at temperatures up to 400°C.

OCIS codes *310.031, 340.7470, 110.39600*

Introduction

Extreme ultraviolet lithography (EUVL) is a leading next generation lithography that operates at an EUV wavelength of 13.4 nm and can print features smaller than 30 nm. Since at

this wavelength all the materials absorb the EUVL systems require vacuum operation. In addition, the optics and the photomask must be coated with reflective multilayer coatings. These multilayer coatings usually consist of Mo and Si layers although more sophisticated structures with diffusion barriers have been proposed to increase their reflectivity and stability.[1,2]

Source power is one of the major roadblocks for achieving the production throughput requirements for EUVL of 100 wafers per hours. However, many source companies are now considering alternate fuels to xenon such as tin or lithium. Preliminary results show substantial increase in the source output over xenon-based sources and the EUVL tool source power requirements seem to be reachable in the near future. Yet new fuels bring also new challenges. In particular, the lifetime of collector optics is of concern due to surface contamination, erosion and diffusion of contaminants from the surface into the multilayers. For some fuel materials keeping the multilayer optics at high temperature is beneficial to mitigate some of these problems, especially surface contamination and diffusion into the multilayer structure. Hence, there is a need for high reflectivity multilayer coatings for normal incidence operation that have a stable reflectivity and bandwidth for long periods of time at high temperatures. The goal of this project was to develop multilayer coatings with a normal incidence reflectivity of >50% at 13.4 nm that are stable for thousands of hours at ~400°C.

Numerous previous studies[1-21] have investigated the thermal stability of Mo/Si multilayers that operate in the EUV region. The multilayers were exposed to high temperatures either to study the kinetics of silicide formation,[3,6,7,12] to control the growth and optimize multilayer fabrication[4, 8, 10, 12] or to reduce stress in the multilayers.[5,13,14,17] Long term thermal stability is important for optics used at synchrotron radiation facilities,[11] x-ray lasers and plasma physics[9] and solar physics.[18] However, structural changes in Mo/Si multilayers due to increased

temperature are also of great importance for EUV lithography applications due to very stringent requirements for reflectance and bandwidth stability and figure errors due to stress changes in the multilayers. For example, it has been shown that the period thickness of Mo/Si multilayers shrinks considerably after annealing at 300°C[9,13,15] but measurable change in EUV reflectivity occurs already at or above 100°C.[14,19] Thermal stability can be substantially improved by the introduction of diffusion barriers such as C,[1,20] B_4C[19,21,22] and SiO_2[24] or by using a different multilayer material pair such as Mo_2C/Si or $MoSi_2$/Si.[8,15,16]

Among the multilayer coatings that have been studied in the past we believe that $MoSi_2$/Si multilayer system is the best candidate to meet the high temperature stability criteria. However, we have found that the reflectivity of this multilayer system at 13.4 nm is only ~44%. In this paper we consider another promising candidate, Mo/SiC, which to our knowledge has not been studied before. Based on bulk properties of Mo and SiC this system should have high temperature stability but also should have higher theoretical[25,26] reflectivity (~56%) than $MoSi_2$/Si. We describe the structure of Mo/SiC multilayers in the as-deposited state and compare it with the structure after annealing over a range of temperatures and annealing times. We present a model explaining thermally-induced structural relaxation observed in Mo/SiC multilayers when exposed to high temperatures, and use this model to predict thermal stability of Mo/SiC coatings at 400°C. Finally, the prediction is compared with the experimental results.

Experimental Techniques

Mo/SiC multilayers were deposited using dc-magnetron sputtering as described elsewhere.[2] The multilayer films consisted of 60 bilayer pairs with a period thickness of ~7.5 nm. This period was intentionally larger to account for period contraction at higher temperature

and to achieve peak reflectance at a wavelength of ~13.4 nm after annealing. In all cases we capped the multilayer with a SiC layer because Mo is known to rapidly oxidize when exposed to the air.[27] The multilayer films were deposited on super-polished Si (100) wafers. Each sample was characterized using a Rigaku x-ray diffractometer at the Cu K_α wavelength at 0.1542 nm, and at EUV wavelengths using the Beamline 6.3.2 reflectometer at the Advanced Light Source.[28] Small angle X-ray diffraction (SAXRD) was used primarily to measure the bilayer period thickness. Large angle X-ray diffraction (LAXRD) was utilized to identify crystallinity and grain size of the individual Mo and SiC layers. Each sample was carefully characterized before and after annealing. Selected samples were imaged in cross section with high-resolution transmission electron microscopy (TEM) and analyzed with selected area electron diffraction to look for structural changes, crystallinity and preferential grain orientation. The TEM was performed on a JEOL 2010 that operated at 200 keV and provided a point-to-point resolution better than 0.2 nm. This microscope was equipped with an Oxford EDS detector and a tilting holder allowing up to 20 degree tilt. The stoichiometry of the SiC layers, which were deposited using an alloy sputtering target, was determined using the Rutherford backscattering (RBS) technique. The RBS measurements were performed with He^{++} ions at 2.275 MeV energy and the RBS spectra were acquired at a backscattering angle of 160° angle with the sample perpendicular to the incident ion beam. To improve C, N and O detection sensitivity and accuracy, we used the nuclear reaction analysis (NRA). In particular, for N, the $^{14}N(d,p)\ ^{15}N$ reaction was used, $^{12}C(d,p)^{13}C$ for C, and $^{16}O(d,p)^{17}O$ for O. Annealing was performed in a commercial vacuum furnace made by HSD Engineering. This custom cold wall vacuum furnace was designed to operate up to 1300°C. The chamber base pressure was typically ~5 x 10^{-8} Torr prior to annealing and increased to ~5x10^{-7} Torr during annealing. The annealing temperature was controlled

within ±2°C with multiple thermocouples. The ramp-up and ramp-down rate was ~5°C/min and this time is not included in the reported annealing time.

Results and Discussion

Rutherford backscattering measurements show that the SiC layers were deposited with the correct stoichiometric composition within 2 at.% accuracy. The as-deposited Mo/SiC multilayer has a bilayer period of 7.5 nm and the normal incidence reflectivity of the as-deposited coatings is 52% at 13.9 nm. Subsequent annealing of the coating at 400°C for 48 hours causes the peak reflectivity to decrease to 48%, and peak wavelength to shift to 13.6 nm. The wavelength shift indicates a thermally induced modification of the multilayer structure.

TEM imaging and selected area electron diffraction (SAED) were performed on the cross-sectional samples of the as-deposited and annealed coatings to characterize the structural transformation. TEM images of the layer structure at the bottom of the stack (next to the substrate) are shown in Figs. 1 and 2 for the as-deposited and annealed samples, respectively. The dark layers are the Mo and the light layers are the SiC. The images do not have sufficient resolution to see the atomic lattice in the layers. However, there are clear Moire's fringes in the Mo layers for both samples that indicate that these layers are polycrystalline. Profiles, shown at the bottom of Figs. 1 and 2, were extracted from TEM images perpendicular to the layers and averaged over a width of ~20 nm in the plane of the layers. These profiles were used to determine the individual layer thicknesses listed in Table I.

It is evident that upon annealing a thermally-activated reaction or interdiffusion causes the Mo layers to grow at the expense of the SiC layers. There is a concomitant contraction of the bilayer spacing of 0.2 nm, which is consistent with the observed shift in the reflectivity peak. We

also see that gamma (thickness of Mo divided by the period thickness) increases upon annealing. The value of 0.6 is too large for achieving optimum reflectivity, and is at least part of the reason that the peak reflectivity has decreased.

The SAED data provides additional information about the thermally-induced structural transformation. The electron diffraction images for the as-deposited and annealed samples are shown in Figs. 3 and 4. The change in the diffraction pattern upon annealing clearly indicates that the structural modification is accompanied by a phase transformation. Line profiles extracted through the SAED images were used to identify the diffraction rings. For the as-deposited sample we took a profile along a line at 45 degrees to the film normal. This was necessary because Mo <110> spots along the film normal were saturated. The profile for the annealed sample was taken along the film normal. The radial position in the profiles was converted to units of the momentum transfer $q=2\pi/d$ using the Mo <110> spots (d=2.225 Å) in the as-deposited sample for calibration. The corresponding profiles are shown at the bottom of Figs. 3 and 4. All of the diffraction spots in the as-deposited sample (Fig. 3) are identified as bcc Mo. This indicates that the Mo layers are polycrystalline and the SiC layers are amorphous in the as-deposited multilayer, a result analogous to the structure of Mo/Si multilayers. The SAED of the annealed sample shows weaker Mo spots and the appearance of a new phase that we identify as cubic SiC. This suggests that the elevated temperature causes the SiC layers to crystallize. Note also in the diffraction pattern of Fig. 4 that the Mo <110> spots along the film growth direction are much weaker than the in-plane spots. This indicates that the crystalline regions of the Mo layers have become thinner in the film growth direction. Since the TEM images show that the thickness of the Mo layers increases upon annealing, we infer that there is some interdiffusion at the layer boundaries that consumes the crystalline Mo, and mixes Mo into the SiC layers. The

Mo-SiC intermixing must result in a net volume decrease (increase in density) to produce the observed bilayer contraction.

Model for Intermixing in Mo/SiC

As described above we noticed that Mo/SiC undergoes a thermally-induced structural transformation upon annealing. When the film is annealed at 400°C a portion of the SiC diffuses into the Mo layer, producing an amorphous Mo-Si-C alloy, and the remaining SiC layer crystallizes. We call this structural transformation the "alpha" stage relaxation. In the following we will present a model to describe this transformation and to predict the time required to complete the alpha stage relaxation in the Mo/SiC multilayer structure.

The final products of the alpha stage are the Mo-Si-C alloy layer and the crystalline SiC layer. We can determine the composition and density of the alloy layer from the TEM measurements of the as-deposited film and a completely reacted film annealed at 400°C for 48 hr. Let the initial and final thicknesses of the SiC layer be $\tau_{SiC(i)}$ and $\tau_{SiC(f)}$. Similarly let the thicknesses of the Mo layer and alloy layer be τ_{Mo} and τ_{MoSiC}, respectively. The thicknesses of these layers as measured by TEM are listed in Table I. The number of Mo atoms per unit area in the as-deposited Mo layer is given by,

$$N_{Mo} = \frac{\tau_{Mo}\rho_{Mo}A}{w_{Mo}} = 2.4\times10^{16}\ \text{atoms/cm}^2 \qquad (1)$$

Here ρ_{Mo} is the mass density (10.2 gm/cm^3), A is Avogadro's number (6.02 x 10^{23}) and w_{Mo} is the atomic weight (95.94 gm/mole). This is also the number of Mo atoms per unit area in the

final Mo-Si-C alloy layer. The number of SiC molecules in the alloy layer is equal to the number removed from the as-deposited SiC layer,

$$N_{SiC} = \frac{(\tau_{SiC(i)} - \tau_{SiC(f)})\rho_{SiC} A}{w_{SiC}} = 4.0 \times 10^{15}\,\text{mol/cm}^2 \qquad (2)$$

Here ρ_{SiC} is the mass density of the SiC layer (3.2 gm/cm^3) and w_{SiC} is the molecular weight (40.1 gm/mole). If we write the composition of the alloy layer as $Mo_\beta(SiC)_{1-\beta}$ then,

$$\beta = \frac{N_{Mo}}{N_{Mo} + N_{SiC}} = 0.85 \qquad (3)$$

The mass density of the alloy layer is then given by,

$$\rho_{MoSiC} = \frac{w_{Mo} N_{Mo} + w_{SiC} N_{SiC}}{\tau_{MoSiC} A} = 9.1\,\text{gm/cm}^3 \qquad (4)$$

There has been some investigation of the tertiary phase diagram of the Mo-Si-C system at high temperatures (>1200°C), and an intermetallic compound of composition Mo_5Si_3C has been identified.[29,30] However, the Mo-rich composition of the alloy layers that we observe is far from this stoichiometry, and could possibly represent the solid solubility limit of SiC in Mo.

Once the composition of the alloy layers is known it is possible to model the effect of the structural transformation on the normal incidence reflectivity of the multilayer coating. We model a multilayer coating that has an as-deposited structure of [Mo(3.5 nm)/SiC(3.5 nm)] x 60.

The calculated normal incidence reflectivity is shown in Fig. 5 as a function of the EUV wavelength. The reflectance peaks at 13.36 nm with a value of 56%. After annealing the multilayer structure is transformed to [$Mo_{0.85}SiC_{0.15}$(4.08 nm)/SiC(2.72 nm)] x 60. As seen in Fig. 5, the reflectance peak shifts to a wavelength of 13.04 nm and decreases to a value of 50%. This prediction is in good agreement with the experimentally-observed decrease in reflectivity upon annealing.

The next step is to develop a model for the kinetics of the "alpha" stage relaxation. We consider the intermixing of the Mo and SiC layers to be a diffusion-limited process. Let w be the width of the interlayer and let the composition of the interlayer be $Mo_{\beta}(SiC)_{1-\beta}$. Then according to Gosele and Tu[31] the rate at which the interlayer width increases is given by,

$$\frac{dw}{dt} = \frac{D(T)}{\beta(1-\beta)w} \tag{5}$$

Here D is the temperature-dependent interdiffusion coefficient, characterized by a pre-factor D_0 and an activation energy E_A:

$$D(T) = D_0 \exp(-E_A / kT) \tag{6}$$

The solution of the rate equation (5) is,

$$w^2 = \frac{2Dt}{\beta(1-\beta)} \tag{7}$$

The crystalline Mo layer shrinks as it is consumed by the growth of the interlayers. The depletion of the Mo layer is related to the width of the interlayers according to,

$$\Delta\tau_{Mo} = 2\beta w \tag{8}$$

The factor of two accounts for the two interlayers on either side of the Mo layer. We combine Eqs. (7) and (8) to obtain,

$$\Delta\tau_{Mo}^2 = 8\frac{\beta}{1-\beta}Dt \tag{9}$$

This equation directly relates the kinetics of the diffusion process to the depletion of the crystalline Mo layers.

The width of the Mo layer can be directly measured using x-ray diffraction (XRD). The polycrystalline Mo has a strong <110> texture in the growth direction. This produces a diffraction peak at $2\theta_{<110>}$ = 40 deg. We can model the profile of the diffraction peak as a Gaussian,

$$I(2\theta) = I_0 \exp\left[-\frac{(2\theta - 2\theta_{<110>})^2}{2\sigma^2}\right] \tag{10}$$

Note that 2σ is the width of the XRD peak in 2θ space, and so has units of radians. The thickness of the crystalline Mo layer is inversely proportional to the peak width according to,[32]

$$\tau_{Mo} = \sqrt{\frac{2}{\pi}} \frac{\lambda}{2\sigma \cos\theta_{<110>}} \tag{11}$$

Here λ is the Cu-Kα x-ray wavelength of 0.1542 nm.

We have studied the kinetics of the alpha stage relaxation in Mo/SiC multilayers by annealing a series of films as a function of time at three different temperatures of 350, 375 and 400°C. XRD measurements are shown in Fig. 6 for the series of annealing times at each temperature. The as-deposited films show only the Mo <110> peak near 2θ = 40 deg. Upon annealing the Mo peak broadens and shifts to smaller angle, while a new peak appears at 2θ = 35 deg corresponding to SiC <111>. This behavior confirms our model for the "alpha" stage relaxation wherein the crystalline Mo layers are consumed and the SiC layers crystallize. The broadening of the Mo <110> peak is due to the decreasing thickness of the Mo layers. The shift is probably due to a lattice strain produced by the compressive stress of the surrounding SiC layers. We fit a Gaussian profile to the Mo <110> peak to determine the width of the Mo layers using Eq. (11). Plotting $\Delta\tau_{Mo}^2$ as a function of time produced a straight line, as shown in Fig. 7. The interdiffusion coefficient is obtained from the slope of the line according to Eq. (9). The resulting values are listed in Table II.

The Arrhenius plot of the temperature dependence, shown in Fig. 8, confirms that the interdiffusion is thermally activated. The best fit line yields an activation energy of E_A = 2.6 eV and a value of D_0 = 0.8 cm^2/s.

Having characterized the kinetics of the diffusion process we can now estimate the time required to complete the "alpha" stage relaxation at any temperature. This is the time required to stabilize the reflectivity of the coating. We assume that the as-deposited structure consists of

pure SiC and crystalline Mo layers having a thickness τ_{Mo}. At elevated temperature the SiC diffuses into the crystalline Mo layer until it is completely consumed. The time to stabilize, t_S, is given by,

$$t_S = \frac{(1-\beta)\tau_{Mo}^2}{8\beta D_0 \exp(-E_A / kT)} \qquad (12)$$

The stabilization time is plotted as a function of temperature in Fig. 9 for the case where the initial Mo layer thickness is τ_{Mo} = 3 nm. It is interesting to note that the large activation energy produces a dramatic decrease in the stabilization time with increasing temperature; the time ranges from 10 trillion years at 100°C to 213 seconds at 500°C.

We tested our model by annealing as-deposited and pre-annealed Mo/SiC multilayer at 500°C for 100 hours. Pre-annealed Mo/SiC multilayer has been previously annealed at 400°C for 100 hours and should have, according to our model, completed the “alpha” stage relaxation. Hence, we should not see any additional reflectivity loss or peak wavelength shift due to the annealing at 500°C for 100 hours. The experimental results, shown in Fig. 10, indicate that there is indeed some additional relaxation of the multilayer structure at 500°C that causes the reflectivity peak to decrease and shift to a slightly shorter wavelength. Hence, we conclude that the “alpha” stage relaxation process is the dominant structural relaxation mechanism at temperatures up to 400°C, but other relaxation processes are activated at higher temperatures. The characterization of these other processes and the stability of Mo/SiC multilayers at temperatures greater than 400°C will be the subject of future studies.

Conclusions

We believe that the alpha stage relaxation studied herein is the dominant structural transformation pathway for the Mo/SiC system at elevated temperatures up to 400°C. The multilayer structure should be relatively stable in this range of operating temperatures after the relaxation process is complete. The crystallization of the SiC layers suggests that the system has reached at least a local thermodynamic equilibrium, which provides a kinetic barrier to further structural transformation at these temperatures. It is likely, however, that exposure to higher temperatures overcomes these kinetic barriers inducing new pathways for structural relaxation in the multilayer film, as the Mo-Si-C layer progresses towards the composition of the equilibrium high temperature phase.

Acknowledgments

This work was performed under the auspices of the U.S. Department of Energy by University of California Lawrence Livermore National Laboratory under contract No. W-7405-Eng-48. The project was funded by Intel Corp and managed by Robert Bristol (Intel Corp.). We would like to thank Jennifer Alameda and Lauren M. Hubner (LLNL) for coating depositions, characterization and annealing, Nhan Nguyen (LLNL) for system control, Andy Aquila, Franklin Dollar and Eric M. Gullikson (LBNL) for reflectivity measurements, and ALS personnel for synchrotron beam.

References

1. H. Takenaka, T. Lawamura, “Thermal stability of Mo/C/Si/C multilayer soft x-ray mirrors”, J. of Elec. Spec. and Rel. Phenom. 80, 381384 (1996).

2. S. Bajt, J. B. Alameda, T. W. Barbee Jr., W. M. Clift, J. A. Folta, B. Kaufmann, E. A. Spiller, “Improved reflectance and stability of Mo-Si multilayers”, Opt. Eng. 41, 1797 (2002).
3. Z. Jiang, X. Jiang, W. Liu, and Z. Wu, “Thermal stability of multilayer films Pt/Si, W/Si, Mo/Si, and W/Si”, J. Appl. Phys. 65, 196-200 (1989).
4. A. Kloidt, K. Nolting, U. Kleineberg, B. Schmiedeskamp, and U. Heinzmann, P. Müller, and M. Kühne, “Enhancement of the reflectivity of Mo/Si multilayer mirrors by thermal treatment”, Appl. Phys. 58, 2601-2603 (1991).
5. R. R. Kola, D. L. Windt, W. K. Waskiewicz, B. E. Weir, R. Hull, G. K. Celler, and C. A. Volkert, “Stress relaxation in Mo/Si multilayer structures”, Appl. Phys. Lett. 60, 3120-3122 (1992).
6. Y. Ijdiyaou, M. Azizan, E. L. Ameziane, M. Brunel, and T. A. Nguyen Tan, “On the formation of molybdenum silicides in Mo-Si multilayers: the effect of Mo thickness and annealing temperature”, Appl. Surf. Scien. 55, 165-171 (1992).
7. R. S. Rosen, D. G. Stearns, M. A. Villiardos, M. E. Kassner, S. P. Vernon, and Y. Cheng, “Silicide layer growth rates in Mo/Si multilayers”, Appl. Opt. 32, 6975-6980 (1993).
8. V. V. Kontradenko, Yu. P. Pershin, O. V. Poltseva, A. I. Fedorenko, E. N. Zubarev, S. A. Yulin, I. V. Kozhevnikov, S. I. Saitov, V. A. Chirkov, V. E. Levashov, and A. V. Vinogradov, ”Thermal stability of soft x-ray Mo-Si and $MoSi_2$-Si multilayer mirros”, Appl. Opt. 32, 1811-1816 (1993).
9. H. Azuma, A. Takeichi, I. Konomi, Y. Watanabe, and S. Noda, “Thermally induced structural modification of nanometer-order Mo/Si multilayers by the spectral reflectance of laser-plasma soft X-rays”, Jpn. J. Appl. Phys. 43, 2078-2082 (1993).

10. J. M. Liang, and L. J. Chen, “Interfacial reactions and thermal stability of ultrahigh vacuum deposited multilayered Mo/Si structures”, J. Appl. Phys. 79, 4072-4077 (1996).
11. E. Ziegler, “Multilayers for high heat load synchrotron applications”, Opt. Eng. 34, 445-452 (1995).
12. H.-J. Voorma, E. Louis, N. B. Koster, and F. Bijkerk, “Temperature induced diffusion in Mo/Si multilayer mirrors”, J. Appl. Phys. 83, 4700-4708 (1998).
13. D. L. Windt, “Stress, microstructure, and stability of Mo/Si, W/Si, and Mo/C multilayer films”, J. Vac. Sci. Technol. A 18, 980-991 (2000).
14. C. Montcalm, “Reduction of residual stress in extreme ultraviolet Mo/Si multilayer mirrors with postdeposition thermal treatments”, Opt. Eng. 40, 469-477 (2001).
15. T. Feigel, H. Lauth, S. Yulin, N. Kaiser, “Heat resistance of EUV multilayer mirrors for long-time applications”, Microelectr. Eng. 57-58, 3-8 (2001).
16. T. Feigl, S. Yulin, T. Kuhlmann, and N. Kaiser, “Damage resistant and low stress EUV multilayer mirrors”, Jpn. J. Appl. Phys. 41, 4082-4085 (2002).
17. T. Leisegang, D. C. Meyer, A. A. Levin, S. Braun, P. Paufler, “On the interplay of internal/external stress and thermal stability of Mo/Si multilayers”, Appl. Phys. A 77, 965-972 (2003).
18. D. L. Windt, S. Donguy, J. Seely, and B. Kjornrattanawanich, “Experimental comparison of extreme-ultraviolet multilayers for solar physics”, Appl. Opt. 43, 1835-1848 (2004).
19. T. Böttger, D. C. Meyer, P. Paufler, S. Braun, M. Moss, H. Mai, E. Beyer, “Thermal stability of Mo/Si multilayers with boron carbide interlayers”, Thin Solid Films 444, 165-173 (2003).

20. H. Takenaka, H. Io, T. Haga, and T. Kawamura, “Design and fabrication of highly heat-resistant Mo/Si multilayer soft x-ray mirrors with interleaved barrier layers”, J. Synchrotron Rad. 5, 708-710 (1998).
21. S, Bajt, “High-reflectance interface-engineered multilayers”, Invited talk at PXRMS’02, Chamonix, France, March 3-7, 2002, http://cletus.phys.columbia.edu/~pxrms/archives/pxrms02/index.html.
22. S. Braun, H. Mai, M. Moss, R. Scholz, A. Leson, “Mo/Si multilayers with different barrier layers for applications as extreme ultraviolet mirrors”, Jpn. J. Appl. Phys. 41, 4074-4081 (2002).
23. A. Patelli, J. Ravagnan, V. Rigato, G. Salmaso, D. Silvestrini, E. Bontempi, L. E. Depero, “Structure and interface properties of Mo/B4C/Si multilayers deposited by rf-magnetron sputtering”, Appl. Surf. Sci. 238, 262-268 (2004).
24. M. Ishino, O. Yoda, H. Takenaka, K. Sano, M. Koike, “Heat stability of Mo/Si multilayers inserted with compound layers”, Surf. Coat. Technol. 169-170, 628 (2003).
25. D. L. Windt, “IMD- software for modeling the optical properties of multilayer films”, Comput. Phys. 12, 360-370 (1998).
26. http://www.cxro.lbl.gov/optical_constants/ managed by E. M. Gullikson.
27. J. H. Underwood, E. M. Gullikson, and K. Nguyen, “Tarnishing of Mo/Si multilayer x-ray mirrors,” Appl. Opt. **32**, 6985-6990 (1993).
28. J. H. Underwood, and E. M. Gullikson, “High-resolution, high-flux, user friendly VLS beamline at the ALS for the 50-1300 eV energy region,” J. Electron Spectrosc. Relat. Phenom. **92**, 265-272 (1998).

29. S. Govindarajan, J. J. Moore and J. Disam, “Synthesis of nanocomposite thin films based on the Mo-Si-C ternary system and compositional tailoring through controlled ion bombardment”, Metall. Mater. Trans. A, **29A**, 1719-1725 (1998).
30. X. Fan, K. Hack and T. Ishigaki, Mat. Sci. Eng. **A278**, 46 (2000).
31. U. Gosele and K. N. Tu, “Growth kinetics of planar binary diffusion couples – thin-film case versus bulk cases”, J. Appl. Phys. **53**, 3252-3260 (1982).
32. W. H. Zachariasen, *Theory of X-ray Diffraction in Crystals*, (John Wiley & Sons, New York, 1945) p. 102.

Tables

TABLE I: Values of the layer thicknesses, bilayer spacing and gamma determined from the TEM images.

Sample	*Mo layer (nm)*	*SiC layer (nm)*	Λ *(nm)*	Γ
As-deposited	3.77	3.73	7.50	0.50
400°C, 48 hr	4.40	2.90	7.30	0.60

Table II: Values of the interdiffusion coefficient determined for the alpha stage relaxation of Mo/SiC multilayers.

Temperature (^{o}C)	*D (cm^2/s)*
350	4.8×10^{-22}
375	2.6×10^{-21}
400	1.8×10^{-20}

Figure Captions

Fig. 1: Cross-sectional TEM image of the as-deposited Mo/SiC multilayer coating. The plot at the bottom shows the layer profile obtained from the image by averaging over ~20 nm in the plane of the layers.

Fig. 2: Cross-sectional TEM image of the Mo/SiC multilayer coating annealed at 400°C for 48 hours. The plot at the bottom shows the layer profile obtained from the image by averaging over ~20 nm in the plane of the layers.

Fig. 3: Small-area electron diffraction pattern for the as-deposited Mo/SiC multilayer coating. The direction normal to the film is vertical. The profile shown at the bottom was taken along the white line.

Fig. 4: Small-area electron diffraction pattern for the annealed Mo/SiC multilayer coating. The direction normal to the film is vertical. The profile shown at the bottom was taken along the white line.

Fig. 5: The normal incidence reflectivity calculated for a 60-period Mo/SiC multilayer coating in the as-deposited state (solid line) and after completion of the alpha stage relaxation (dashed line).

Fig. 6: X-ray diffraction measurements of the Mo/SiC multilayer films annealed for a series of times at temperatures of 350, 375 and 400°C. The as-deposited films show a strong Mo <110>

peak at 2θ = 40 deg. The peak broadens and shifts to lower angle with increasing annealing time. The crystallization of the SiC layers is indicated by the appearance of the SiC <111> peak at 2θ = 35 deg.

Fig. 7: Plots showing a linear relationship between the square of the decrease in the Mo layer thickness and the annealing time. The slope of the line is proportional to the interdiffusion coefficient.

Fig. 8: An Arrhenius plot showing the temperature dependence of the measured interdiffusion coefficient. The slope of the line is the activation energy and the ordinate intercept is D_0.

Fig. 9: The predicted temperature dependence of the stabilization time, defined as the time required to complete the alpha stage relaxation in the Mo/SiC multilayer structure. Here we have assumed that the initial thickness of the crystalline Mo layers is 3 nm.

Fig. 10: Reflectivity and wavelength change due to 100 hour anneal at 500°C. Two pieces of the same coating have been characterized with reflectometer before and after annealing. One piece has been initially cured for 100 hours at 400°C. Both pieces were then annealed at 500 hours for a cumulative time of 100 hours (1 hr + 9 hrs + 90 hrs). Independent of the procedure both pieces ended up having the same final reflectivity and wavelength.

Figures

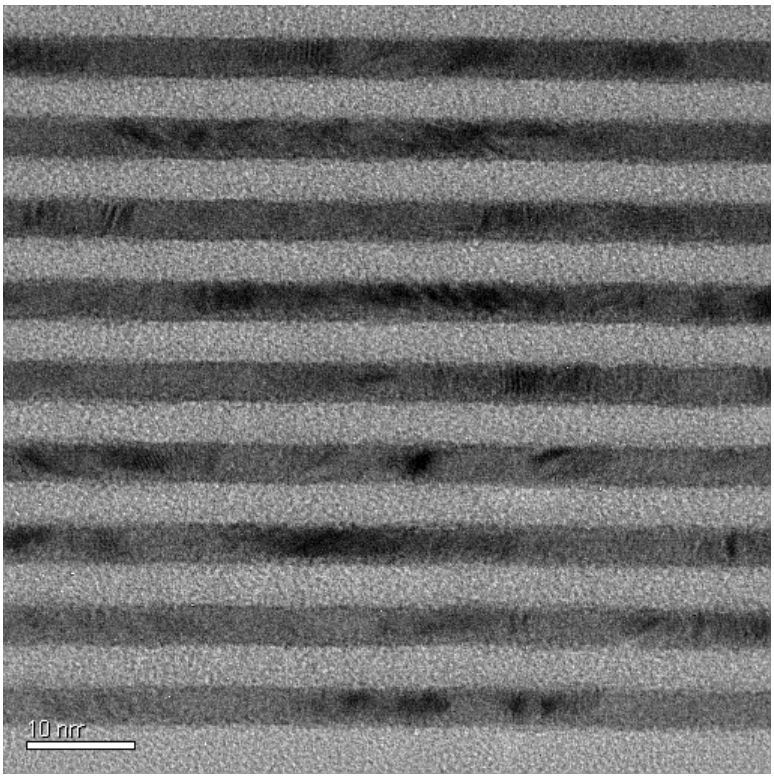

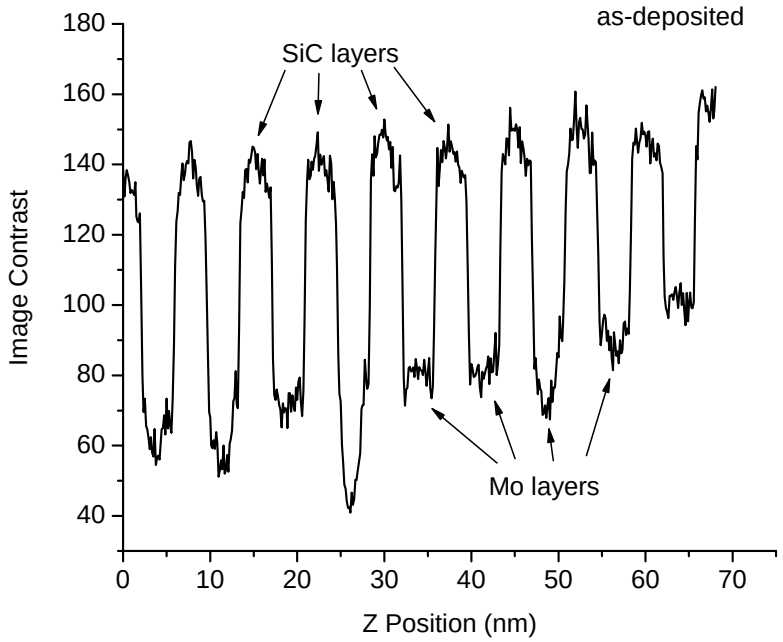

Fig. 1

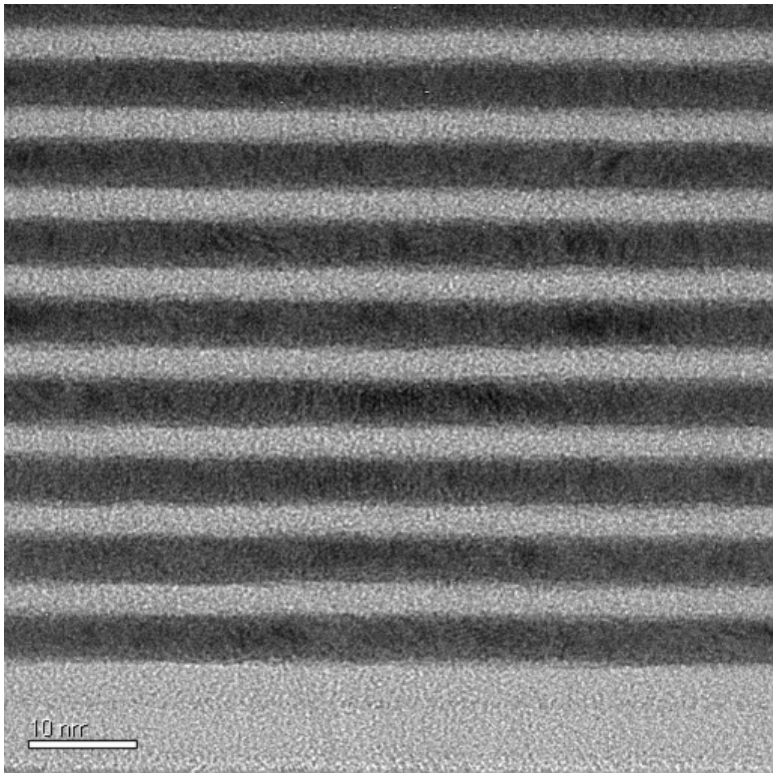
10 nm

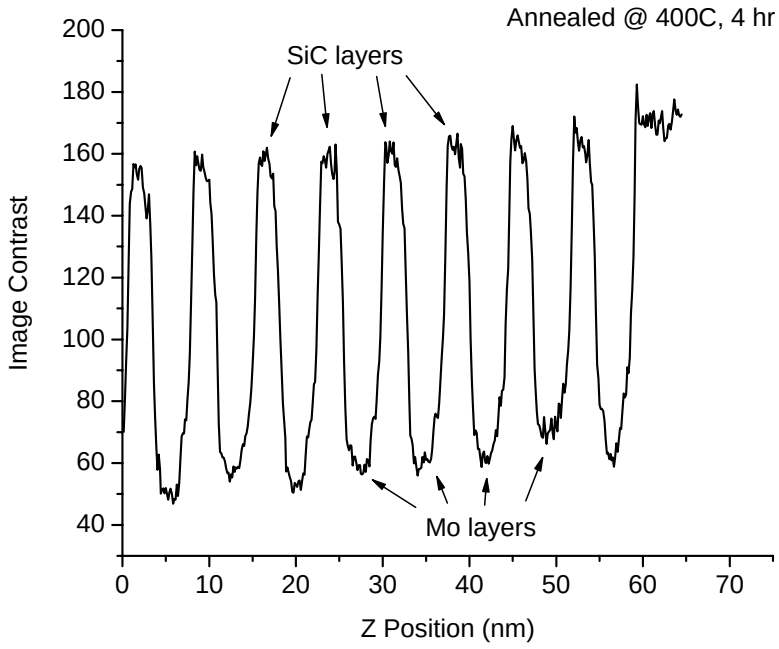
Annealed @ 400C, 4 hr
SiC layers
Mo layers
Image Contrast
Z Position (nm)
200
180
160
140
120
100
80
60
40
0
10
20
30
40
50
60
70

Fig. 2

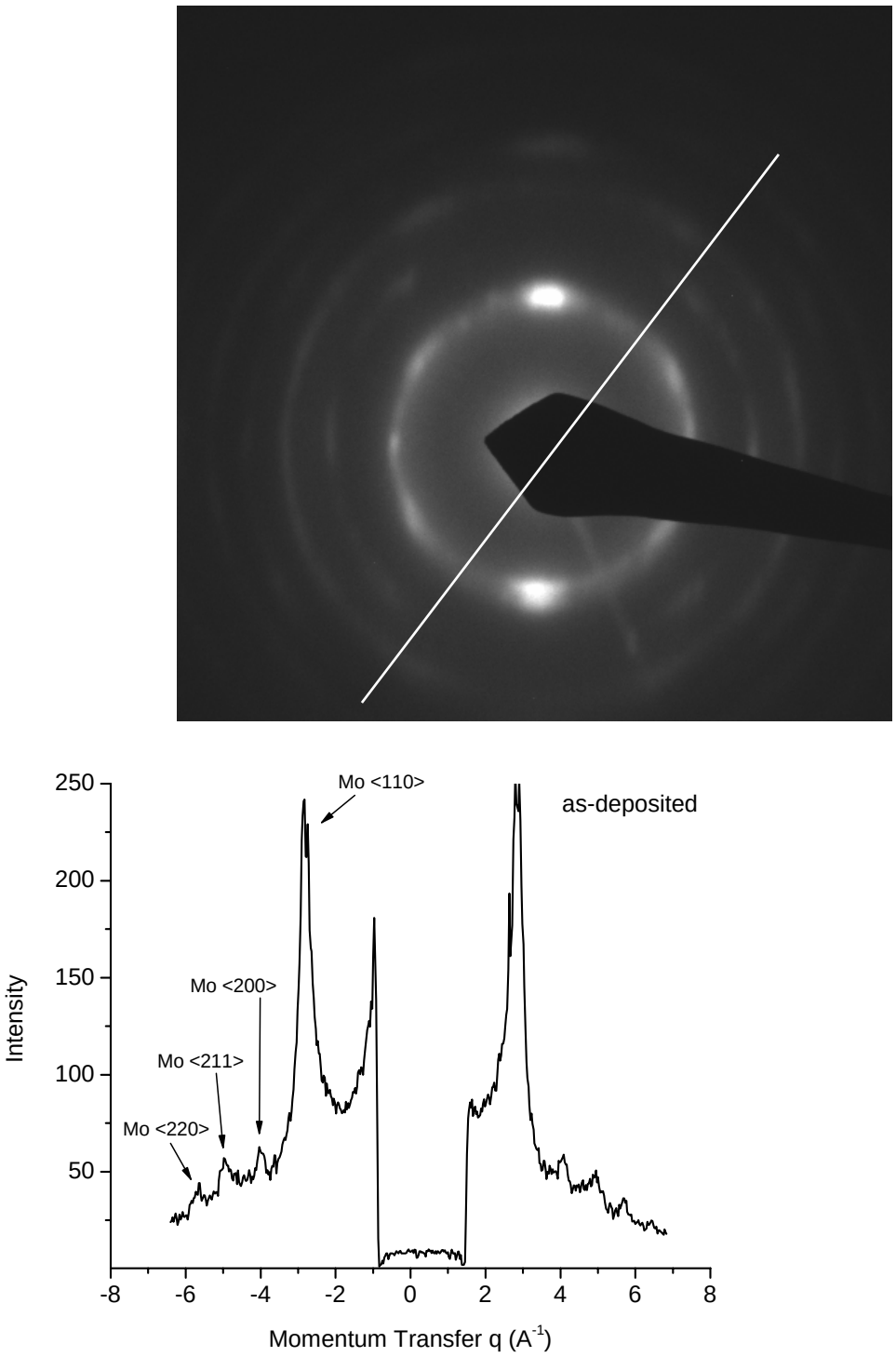
Mo <110>
as-deposited
Mo <200>
Mo <211>
Mo <220>
Intensity
250
200
150
100
50
-8
-6
-4
-2
0
2
4
6
8
Momentum Transfer q (A-1)

Fig. 3

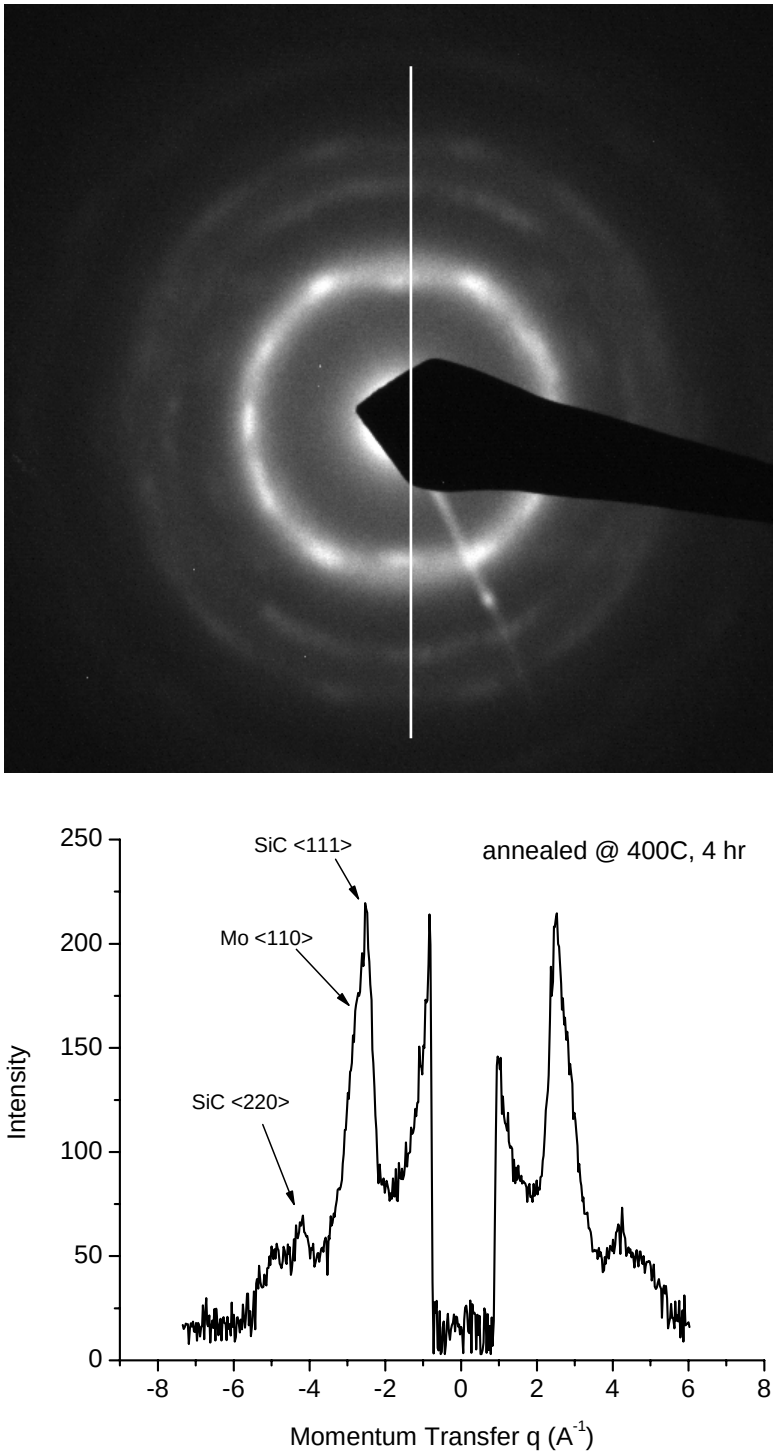
SiC <111>
annealed @ 400C, 4 hr
Mo <110>
SiC <220>
Intensity
250
200
150
100
50
0
-8
-6
-4
-2
0
2
4
6
8
Momentum Transfer q (A-1)

Fig. 4

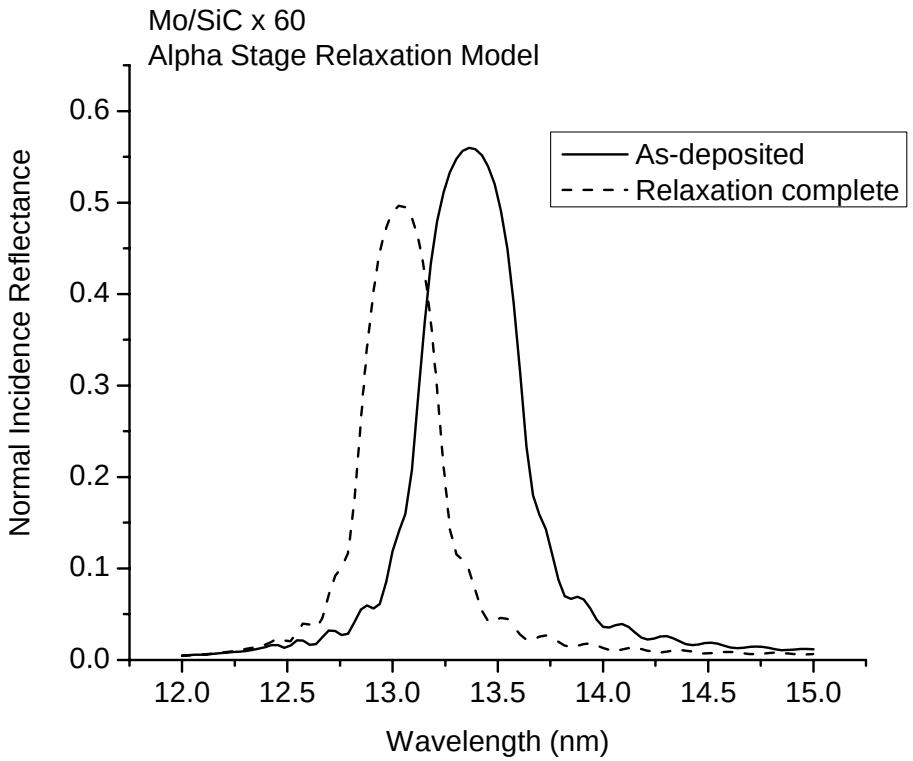
Mo/SiC x 60
Alpha Stage Relaxation Model
As-deposited
Relaxation complete
Normal Incidence Reflectance
0.0
0.1
0.2
0.3
0.4
0.5
0.6
12.0
12.5
13.0
13.5
14.0
14.5
15.0
Wavelength (nm)

Fig. 5

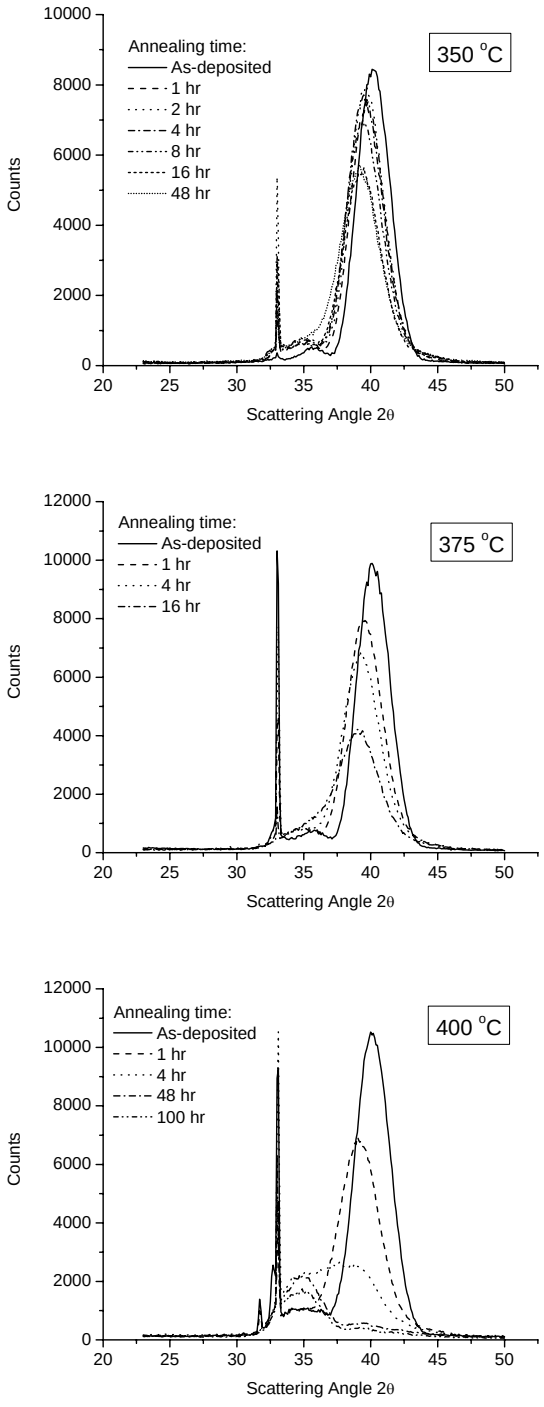
Annealing time:
As-deposited
1 hr
2 hr
4 hr
8 hr
16 hr
48 hr
350 °C
Counts
Scattering Angle 2θ
Annealing time:
As-deposited
1 hr
4 hr
16 hr
375 °C
Counts
Scattering Angle 2θ
Annealing time:
As-deposited
1 hr
4 hr
48 hr
100 hr
400 °C
Counts
Scattering Angle 2θ

Fig. 6

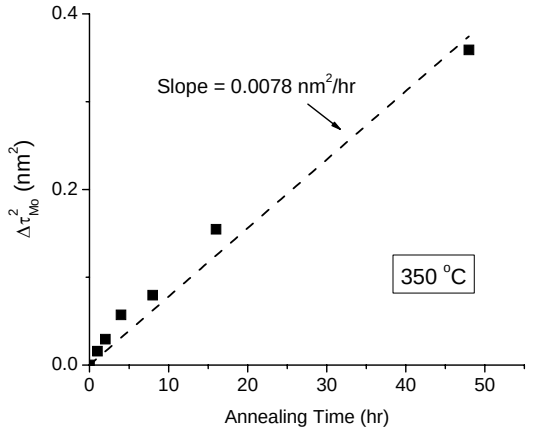
Slope = 0.0078 nm^2/hr
350 ^{o}C
$\Delta\tau^2_{Mo}$ (nm^2)
Annealing Time (hr)

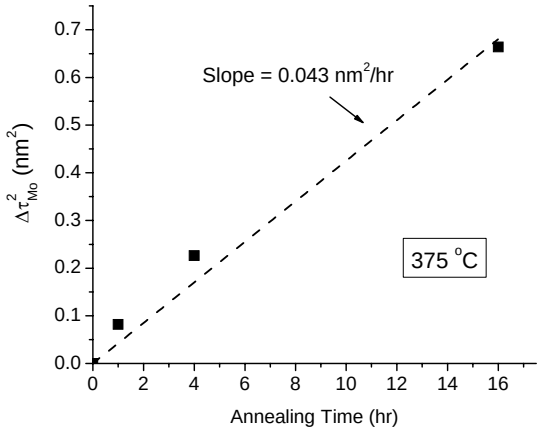
Slope = 0.043 nm^2/hr
375 ^{o}C
$\Delta\tau^2_{Mo}$ (nm^2)
Annealing Time (hr)

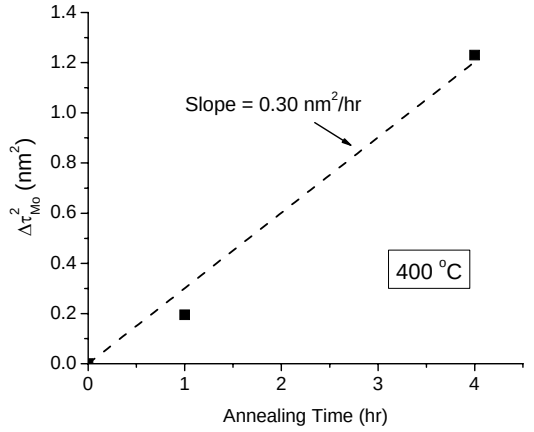
Slope = 0.30 nm^2/hr
400 ^{o}C
$\Delta\tau^2_{Mo}$ (nm^2)
Annealing Time (hr)

Fig. 7

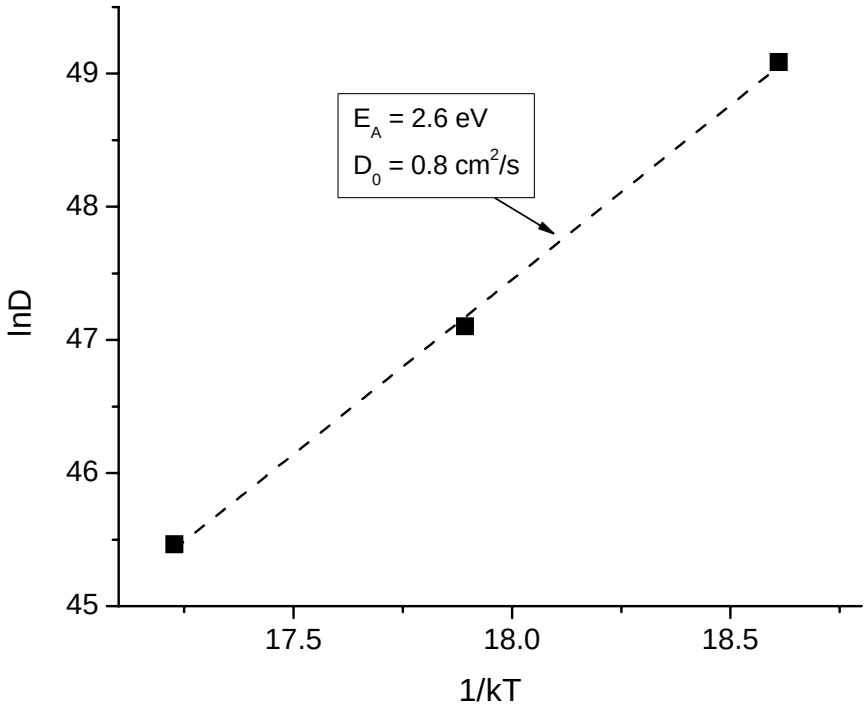

Fig. 8

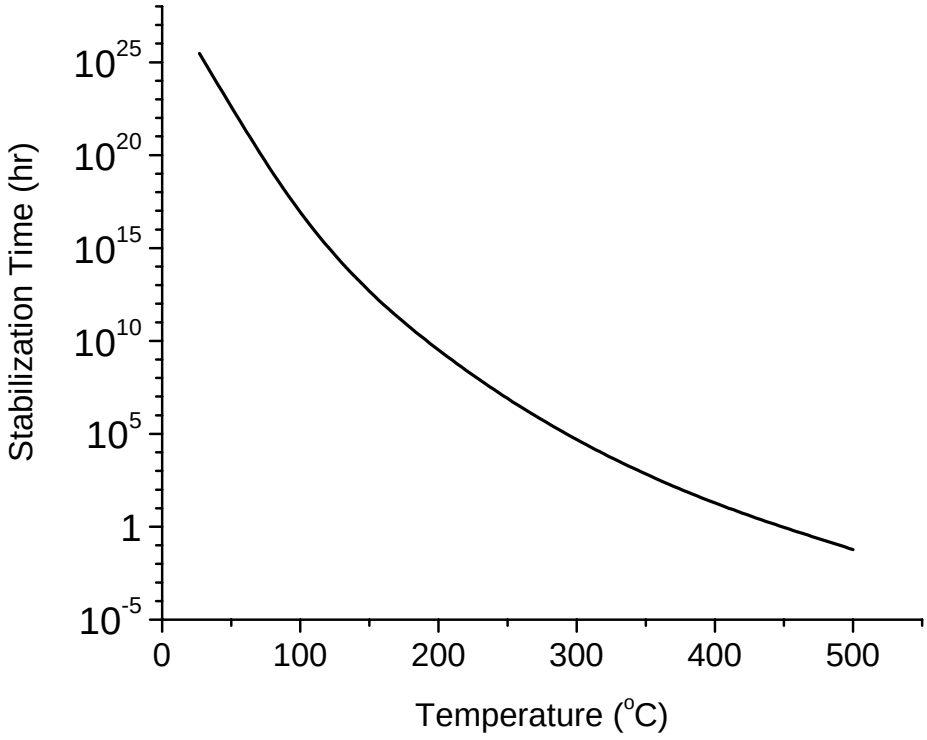
Stabilization Time (hr)
10^25
10^20
10^15
10^10
10^5
1
10^-5
0
100
200
300
400
500
Temperature (°C)

Fig. 9

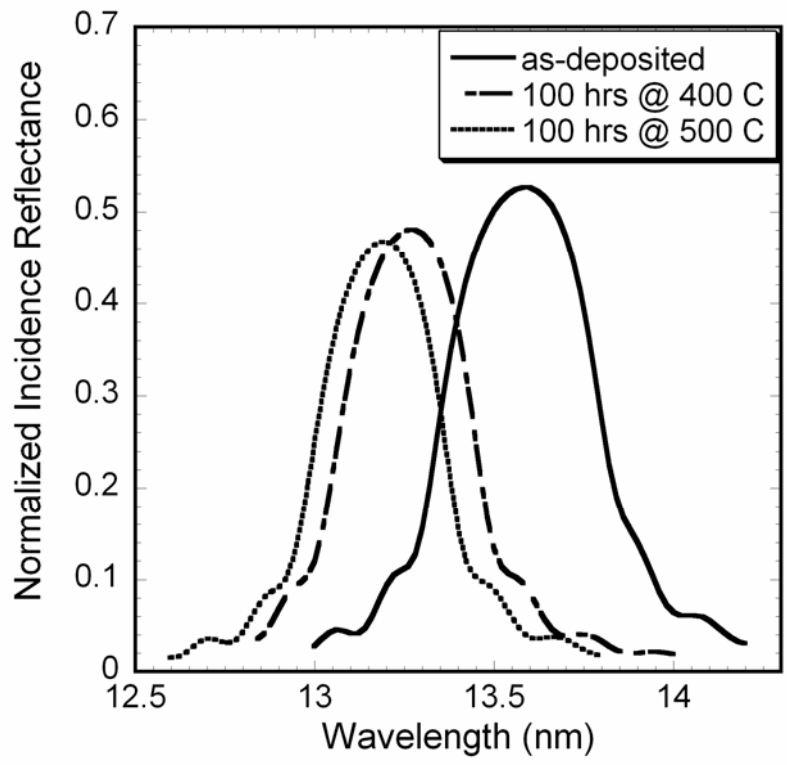
as-deposited
100 hrs @ 400 C
100 hrs @ 500 C
Normalized Incidence Reflectance
0.7
0.6
0.5
0.4
0.3
0.2
0.1
0
12.5
13
13.5
14
Wavelength (nm)

Fig. 10